Characterization of 6.1 Å III-V materials grown on GaAs and Si: a comparison of GaSb/GaAs epitaxy and GaSb/AlSb/Si epitaxy.

A. P. Craig[1*], P. J. Carrington,[2] H. Liu[2] and A. R. J. Marshall[1]
[1]*Physics Department, Lancaster University, Lancaster, LA1 4YB, United Kingdom.*
[2]*Department of Electronic and Electrical Engineering, University College London, Torrington Place, London, WC1E 7JE, United Kingdom.*

Abstract: GaSb *p-i-n* photodiodes were grown on GaAs and Si, using interfacial misfit arrays, and on native GaSb. For the samples grown on GaAs and Si, high-resolution transmission electron microscopy images revealed interface atomic periodicities in agreement with atomistic modeling. Surface defect densities of ~1×10^8 cm^{-2} were measured for both samples. Atomic force microscopy scans revealed surface roughnesses of around 1.6 nm, compared with 0.5 nm for the sample grown on native GaSb. Dark current and spectral response measurements were used to study the electrical and optoelectronic properties of all three samples.

KEYWORDS: A1 Atomic Force Microscopy; A1 Defects; A1 High-resolution X-ray diffraction; A1 interfaces; A3 Molecular Beam Epitaxy; B1 Antimonides

*email: a.craig1@lancaster.ac.uk, phone +44 (0)7971 610832

Sb-based materials offer a wide range of direct bandgaps and are of increasing interest for use in LEDs, lasers and detectors operating in the short- and mid-wave infrared spectral ranges (SWIR, MWIR).[1-4] Applications in fast and low power electronic devices are also possible, owing to high electron mobilities. The growth of Sb-based materials onto lattice-mismatched substrates has attracted much attention in recent years. Various approaches have been used to transition the lattice constant to 6.1 Å. These include metamorphic buffer layers, compositional grading and superlattice layers, among others. Growth of high-quality InAs layers on GaAs substrates has also been demonstrated.[5] In this work, interfacial misfit (IMF) arrays were used to grow GaSb *p-i-n* diodes onto lattice mismatched substrates. The IMF array is a method for molecular beam epitaxial (MBE) growth, reportedly allowing high quality, relaxed epilayers to be deposited directly onto lattice mismatched substrates without the need for a thick metamorphic buffer.[6,7] Strain relief should occur within a few monolayers of the interface via a periodic, self-ordered network consisting of 90° edge dislocations, propagating laterally, rather than into the overlying epilayer. In particular, significant attention has been paid to the growth of GaSb on Si substrates. Thin AlSb buffer layers have been shown to promote the growth of improved-quality GaSb epilayers, through a mechanism of action thought to result from the creation of small islands of AlSb acting as sites where 2D growth is energetically favoured.[8-11] In addition, various groups have already demonstrated III-V lasers on Si substrates.[12-15] Ultimately, growth of Sb-based materials on Si offers the possibility to integrate mid-infrared sources and detectors with CMOS circuitry. The marriage of III-V infrared sources and detectors with "lab-on-a-chip" technology could also allow for diagnostic applications in biomedicine.[16] On the other hand, selection of a GaAs substrate offers reduced cost and proven Ohmic contacts, as well as the possibility to integrate MWIR sources and detectors with GaAs electronics. A variety of IMF-array-based devices have already been demonstrated on GaAs, including Sb-based lasers,[17] LEDs[18] and photodiodes.[19] Both GaAs and Si substrates are also optically transparent in the MWIR: a significant additional benefit for flip-chip mounting focal plane arrays. Although a substantial body of work already exists examining the structural properties of mismatched epitaxial layers, there exist relatively few reports presenting device-level characterization and comparisons between GaSb/GaAs and GaSb/ AlSb/Si epitaxy.

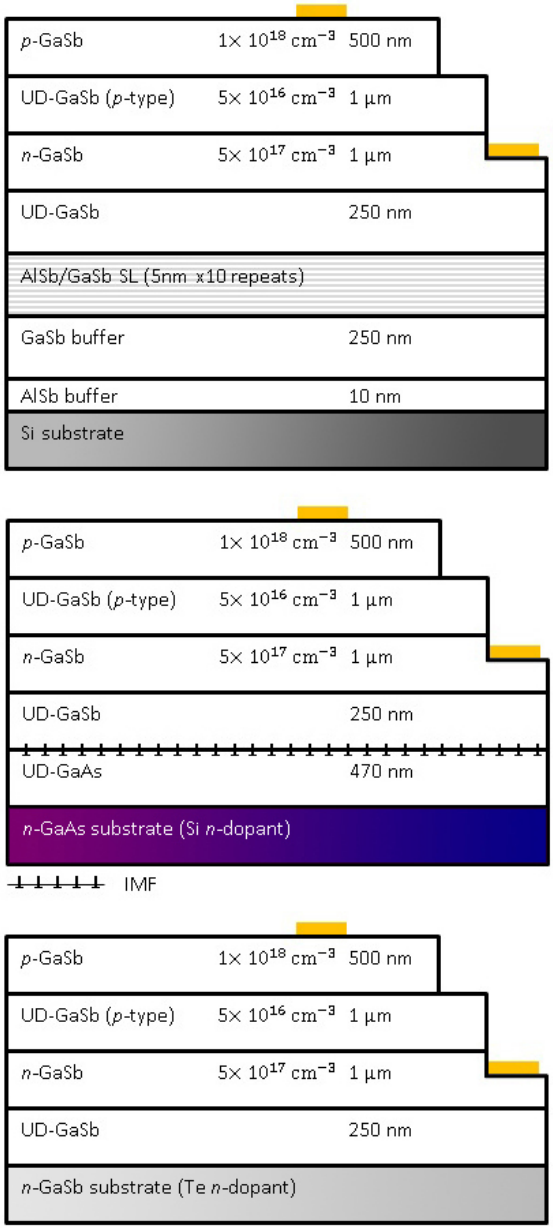

Figure 1: Shows layer profiles for the three samples. The uppermost three layers form a GaSb *p-i-n* structure, which is common to the three samples.

The above noted strong scientific and technological interest motivated the study presented here. Using x-ray diffraction (XRD), atomic force microscopy (AFM), transmission electron microscopy (TEM) and dark current measurements, GaSb *p-i-n* structures grown on GaAs and Si substrates using IMF arrays were compared with an equivalent structure grown lattice matched on native GaSb.

Layer profiles for the three samples are shown in Figure 1. The samples were grown by solid-source MBE. Thermal effusion K-cells provided Ga and Al fluxes, whilst As_2 and Sb_2 fluxes were provided by valved cracker cells. *In-situ* reflection high energy electron diffraction (RHEED) was used to dete-

rmine the growth rates and to monitor surface reconstruction. In addition, the substrate temperature was calibrated using a temperature-dependent GaSb RHEED transition in each case, in order to achieve a GaSb growth temperature (of 510 °C) for all three samples. In order to ensure identical MBE chamber conditions, the growths were also carried out consecutively. For the sample grown on Si, a wafer miscut at 4° to [110] was used in order to reduce the formation of anti-phase domains (APDs) during the growth of the GaSb overlayer. The native oxide layer was first removed by holding the Si substrate at a temperature of 900 °C for 10 minutes. Then the substrate was next cooled down to 400 °C for the growth of the 10 nm AlSb nucleation layer. The temperature was then reheated to 510 °C for the growth of the GaSb buffer layer and the 10 period 5nm AlSb/5nm GaSb superlattice (SL). The SL acts to force additional strain, causing threading dislocations originating at the Si interface to travel and recombine with each other, improving the material quality in the electrically active GaSb layers. For the sample grown on GaAs, oxide desorption was carried out at 600 °C, and a GaAs buffer layer was then deposited at 0.7 MLs^{-1} and 570 °C (with 2 MLs^{-1} As_2 overpressure). The IMF interface was subsequently initiated, through a short pause without incident As_2 flux, followed by the application of Sb_2 flux. The formation of an IMF array was confirmed by the observation of a 2×8 RHEED pattern, and GaSb growth then proceeded. For the sample grown on native GaSb, oxide desorption was carried out at 560 °C before GaSb overgrowth. For all three samples, the *p*-type dopant was Be and the *n*-type dopant was GaTe. The GaSb growth rates were all 0.8 MLs^{-1} and the Sb_2 overpressure was 1.7 MLs^{-1} (the V-III ratio was 2.1). XRD was carried out using a Bede QC200 Diffractometer. AFM was carried out in tapping-mode using a Veeco Multi-mode scanning probe microscope (SPM). Cross-sectional TEM was carried out for the samples grown on GaAs and Si, using a JEOL 2000 FX. In processing, annular top contacts were evaporated first, using Ti/Au. Circular mesas were then defined using $HCl:H_2O_2:H_2O$ (1:1:5). Finally, the lower contact was made to the doped *n*-GaSb layer, using AuGe/Au. Dark current measurements were carried using a Keithley 2400 SourceMeter®. An Oxford Instruments cryostat was used for low temperature measurements. Spectral response measurements were carried out using a Bentham TMc 300 Monochromator in

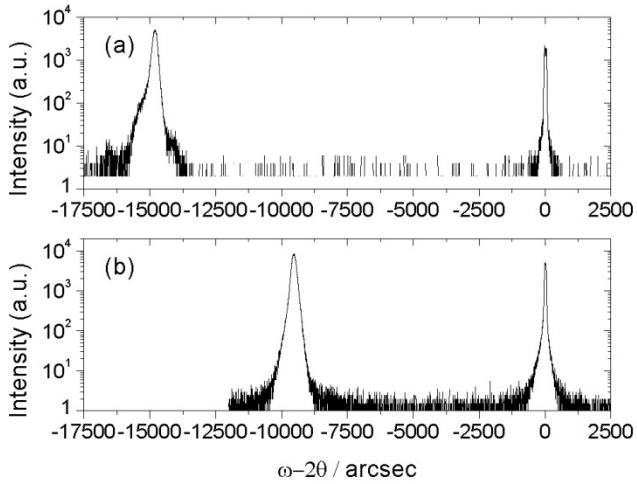

Figure 2: XRD data (a) for the sample grown on Si and (b) for the sample grown on GaAs.

combination with an Oriel tungsten filament lamp.

XRD scans for the sample grown on Si and the sample grown on GaAs are shown in Figure 2. For the sample grown on Si, the 14,860 arcsec angular separation corresponds to 98.2% relaxation of the GaSb epilayer. The features to the left hand side of the GaSb peak (at around -15,300 arcsec) result from the AlSb buffer and SL layers. For the sample grown on GaAs, the angular separation was 9,561 arcsec, corresponding to 99.7% relaxation of the overlying GaSb epilayers. Full-widths-at-half-maximum (FWHM) were calculated to be ~180 arcsec for both the sample grown on Si and the sample grown on GaAs, whereas the sample grown on GaSb (not shown) yielded a value of 107 arcsec. This indicates superior material quality for the lattice-matched growth, as expected. It should be noted that, while the FWHM values measured depend on the optics of the Bede QC200 XRD system – i.e. a direct comparison cannot be drawn with FWHM measured using other equipment – the values noted above were still comparable with one another, allowing for an assessment of relative material quality.

AFM scans (10×10 μm) for all three samples are shown in Figure 3. The RMS roughness was calculated in each case, and found to be ~1.6 nm for both the sample grown on Si and the sample grown on GaAs, and ~0.5 nm for the sample grown on native GaSb. It was noted that no atomic steps due to the miscut substrate were observed in (a). This was attributed to the separation of the step edges (calculated to be ~9 nm) being smaller than the radius of the AFM tip (approx. 10 nm), i.e. these features were perhaps present but not resolved. However, the planar macroscopic topology of this

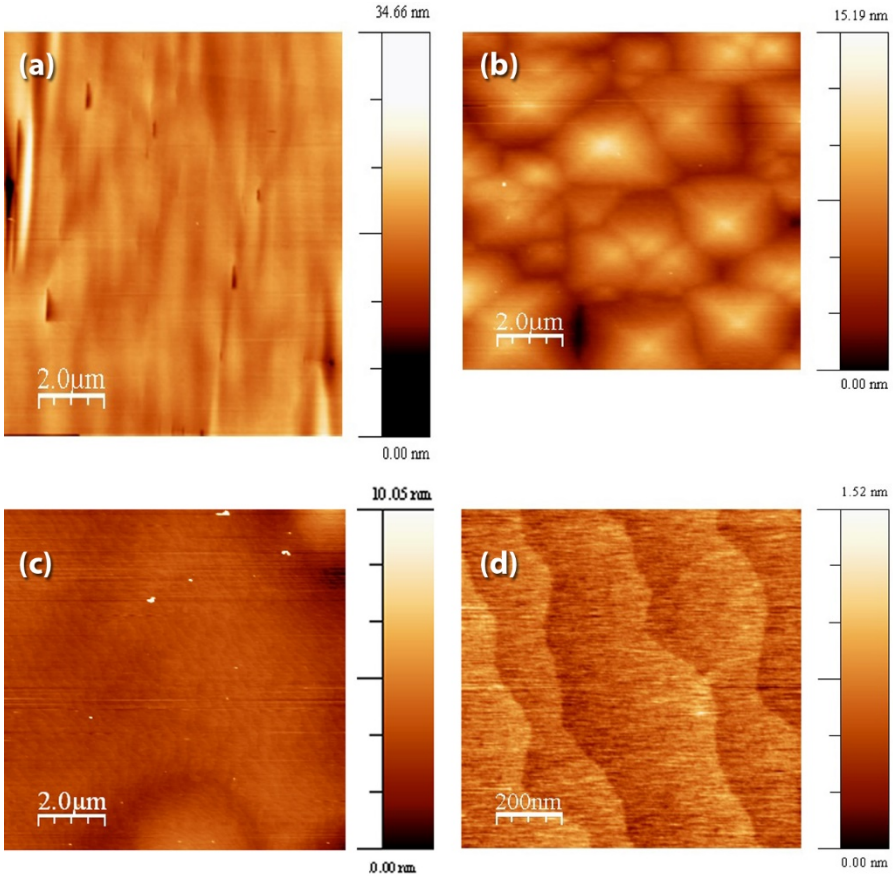

Figure 3: AFM scans for 10 x 10 µm areas of (a) the sample grown on Si, (b) the sample grown on GaAs, and (c) the sample grown on native GaSb. Part (d) shows a 1 x 1 µm scan for the sample grown on GaSb.

sample is clearly evidenced. It was further noted that the hillocks visible in (b) have an appearance similar to features reported previously for GaSb layers grown on GaAs by metal organic vapor phase epitaxy (MOVPE).[20] Finally, Figure 3(d) gives a 1×1 µm scan for the sample grown lattice matched to GaSb, providing further detail to Figure 3(c).

Figure 4 (a) and (b) show cross-sectional TEM images of the sample grown on Si. Inspecting part (a), it can be seen that the atomic arrangement at the interface forms an IMF array: a self-ordered, repeating pattern consisting of 8 lattice sites of the AlSb buffer meshed with 9 lattice sites of the Si substrate. The additional lattice site in the AlSb layer is accommodated by a 90° misfit dislocation. This periodicity arises directly from the ratio a_e:a_s, where a_e is the lattice constant of the buffer layer and a_s is the lattice constant of the substrate. Part (b) shows the same interface at 5000x magnification. Based upon counting threading dislocations in tilted cross-sectional images (where the area captured is known) the threading dislocation density was estimated to be $\sim 1 \times 10^8$ cm^{-2}. The filtering effect of the AlSb/

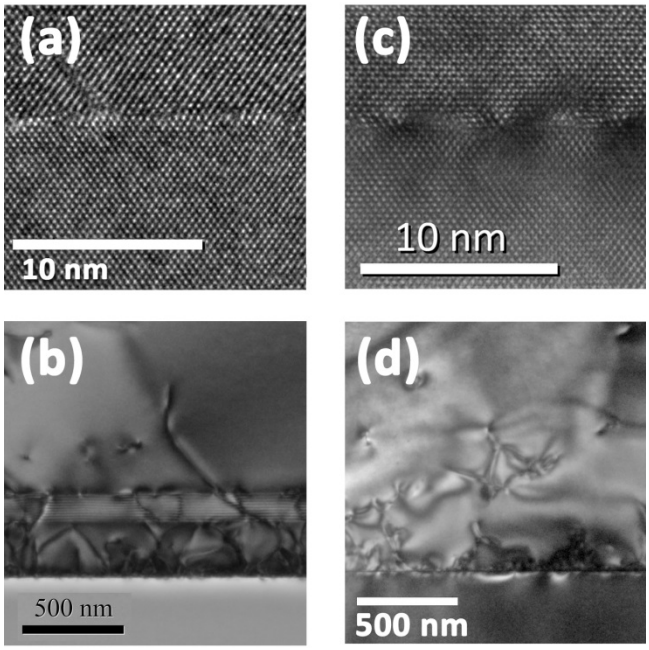

Figure 4: Cross-sectional TEM images of the samples grown on Si and GaAs. Parts (a) and (c) show high magnification views of the interface, for the sample grown on Si and the sample grown on GaAs, respectively. Parts (b) and (d) show the same interfaces at lower (5000x) magnification.

GaSb SL in the sample grown on Si is clearly evident since the threading dislocation density is reduced by more than two orders of magnitude (from ~1×10^{10} cm^{-2} at the AlSb/Si interface). Figures 5 (c) and (d) present a similar analysis for the sample grown on GaAs. This time, the periodicity of the lattice is 13:14, in correspondence with the ratio of the lattice constants of GaSb and GaAs. Again, the threading dislocation density was found to be ~1×10^{8} cm^{-2}. Since the measured surface defect densities were similar for the sample grown on GaAs and the sample grown on Si, the use of the AlSb/GaSb SL seems to have reduced the defect density of the latter to a level similar to the former. However, one remaining question is why the defect density for the growth on Si is inferior before the introduction of the SL. It is proposed that this is due to the fact that there are small differences between the array periods (8:9 for AlSb/Si and 13:14 for GaSb/GaAs) and the ratios of the lattice constants (of AlSb/Si and GaSb/GaAs). For the case of AlSb/Si the 8:9 arrangement leads to a period of 49.08 Å in the AlSb lattice, but only 48.88 Å in the Si lattice, i.e. there is a discrepancy of ~0.2 Å for each array period.[21] On the other hand, for GaSb/GaAs the discrepancy is smaller (~0.1 Å).

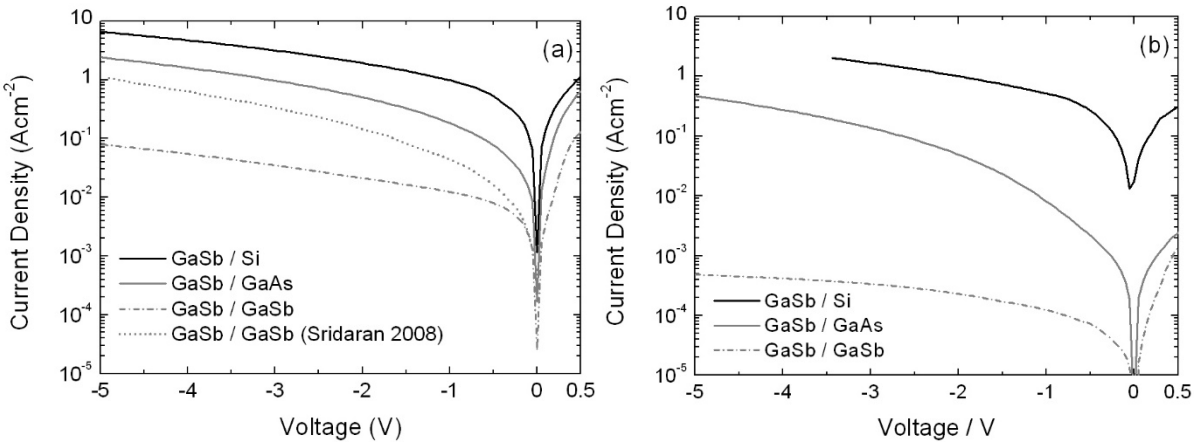

Figure 5: Dark current densities for all three samples. Part (a) shows 300 K data for 400 μm diameter mesas. Part (b) shows data at 120 K for 800 μm diameter mesas. Data from [22] is also shown in (a), providing a comparison with GaSb *p-i-n* diodes reported in the literature.

It is therefore proposed that the smaller value for the additional spacing for the sample grown on GaAs explains the reduced number of defects originating from the interface. It is further proposed that these small additional spacings lead to cumulative strain over the macroscopic scale, relieved by 60° misfits as were exhibited in Figure 4(b/d). It should also be noted that thermal expansion will exacerbate this effect during growth.

Figure 5(a) shows 300 K dark current measurements for all three samples. It can be seen that the lowest dark currents measured were for the sample grown on native GaSb – approximately 0.01 Acm^{-2} at -1.0 V. Our values are similar to, or better than, those for homoepitaxial GaSb *p-i-n* diodes reported elsewhere (an example is shown in the figure).[22] The dark currents for the sample grown on GaAs and the sample grown on Si were both significantly greater: at -1.0 V, currents of approximately 0.18 Acm^{-2} and 0.9 Acm^{-2}, were measured, respectively. It is interesting to note that significantly lower dark currents were observed in the sample grown on GaAs than in the sample grown on Si, suggesting higher material quality in the GaSb/GaAs sample. This contrasts with the TEM analysis, which found that the two samples had a similar dislocation density. It therefore appears that a factor other than the threading dislocation density is responsible for the inferior dark current performance of the sample grown on Si. One explanation is the formation of APDs: these could propagate into the electrically active layers impact the electrical performance of this sample to some extent.[23,24]

Although APDs were not observed directly in the preceding analysis of TEM, their presence is known for III-V (polar) layers on Si (non-polar), with other authors reporting a dependence on the miscut angle, e.g. for 5° a figure of $\sim 5 \times 10^7$ cm^{-2} was reported.[25] It is further noted that the AlSb/GaSb SL layers should not directly affect the electrical performance of the device (other than via a reduction in the threading dislocation density) since a top-top contact scheme was used (the lower contact was to the *n*-type GaSb layer). Approximate area scaling of the dark currents was observed for all three samples, so that bulk leakage currents were established to be dominate (rather than surface leakage currents). Figure 5(b) further shows JV curves at 120 K taken for all three samples. It is immediately apparent that the dark currents for the sample grown on native GaSb have been reduced by several orders. At -1.0 V the dark current density was 1.2×10^{-4} Acm^{-2} whereas, for the samples grown on GaAs and Si, respectively, the dark current densities were measured (again, at -0.1 V) to be 0.51 Acm^{-2} and 8×10^{-3} Acm^{-2}. There was therefore a decrease in the dark current density at low temperature by a factor of ~80 for the sample grown on GaSb, but only by a factor of 2 for the sample grown on GaAs and just a factor of ~1.7 for the sample grown on Si. It is proposed that a trap assisted tunneling process, as exacerbated by the threading dislocation density, is responsible for the weak temperature dependence for the lattice-mismatched samples.

Figure 6 shows the spectral response for all three samples, together with fitted curves, generated by following the approach of Sze.[26] By varying the electron diffusion length parameter to fit the modeled curves to the experimental data, values of 0.2 μm, 0.65 μm and 1.4 μm were extracted, for the sample grown on Si, the sample grown on GaAs and the sample grown on native GaSb, respectively. It is noted that, since the diffusion length is a function of material quality, these spectral response measurements indicate superior material in the sample grown on GaAs compared to the sample grown on Si. This is in agreement with the foregoing analysis of dark current measurements. For all three samples, the modelled hole diffusion length and surface recombination velocity (at the contacts) were fixed at 0.1 μm and 1×10^8 cms^{-1}, respecitvely. It is also observed that the experimental cut-off wavelengths are slightly blue-shifted from the modelled data. This was attributed to the presence of a residual doping level in the intrinsic region of our devices, causing a Moss Burstein shift. The shift was

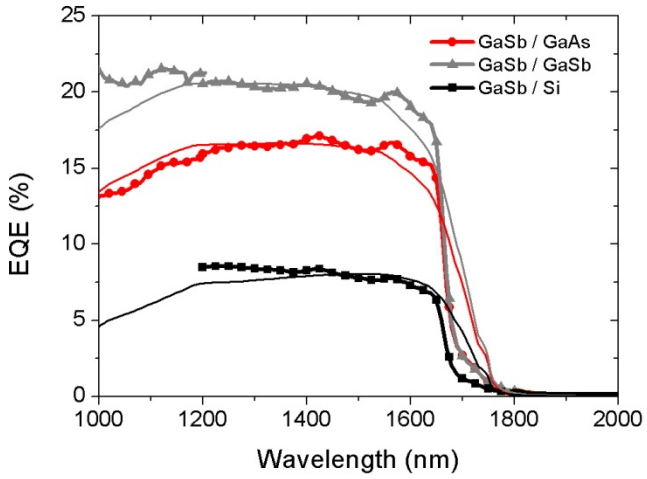

Figure 6: Spectral external quantum efficiency (EQE) measurements for all three samples (line and symbol) and compared with modeled curves (solid lines).

calculated to be ~20 meV which, based on a Fermi Energy calculation, is approximately that expected for a doping level of $3 \times 10^{16} \mathrm{cm}^{-3}$. By comparison, unintentionally doped GaSb layers grown by MBE are known to be *p*-type with a carrier concentration of at least $\sim 1.2 \times 10^{16}\ \mathrm{cm}^{-3}$.[27]

In summary, GaSb *p-i-n* structures were grown on Si and GaAs using IMF arrays and, for comparison, the same structure was grown on native GaSb. Analysis was carried out based on XRD, AFM, TEM, dark current and spectral response measurements. TEM and AFM measurements found similar threading dislocation densities and surface roughnesses, respectively, for the samples grown on Si and GaAs. However, larger dark current densities and reduced quantum efficiencies were still found for both samples, when compared with the lattice matched case. Furthermore, the electrical performance of devices grown on Si was found to be inferior to that for devices grown on GaAs. It is particularly worthy of note that TEM showed the use of an AlSb/GaSb SL layer to be effective in filtering threading dislocations for the sample grown on Si, and that a similar approach could be used for growths on GaAs in order to further refine the crystalline quality achievable, and so to create devices exhibiting lower dark current densities.

198 The authors wish to thank the UK Engineering and Physical Sciences Research Council for the
199 studentship provided to A. P. Craig (grant number EP/P505585/1), the Royal Academy of Engine-
200 ering for the fellowships awarded to A. R. J. Marshall (grant number EP/H043993/1) and P. J. Carrin-
201 gton and the Royal Society for the fellowship awarded to H. Liu.

202

References

[1] A. Krier, M. Yin, V. Smirnov, P. Batty, P. J. Carrington, V. Solovev and V. Sherstnev, Phys. Stat. Sol. (a), 205, No. 1, 129 (2008).

[2] H. H. Gao, A. Krier, and V. Sherstnev, J. Phys. D, Appl. Phys. 32, 1768–1772 (1999).

[3] M Aydaraliev, N V Zotova, S A Karandashov, B A Matveev, N M Stus' and G N Talalakin, Semicond. Sci. Tehcnol. 8, 1575 (1993).

[4] A. Krier and Y. Mao, Infrared Phys and Technol, 38, 397 (1997).

[5] A. Trampert, E. Tournié and K. H. Ploog, Appl. Phys. Lett 66, 17 (1995).

[6] S. Huang, G. Balakrishnan and D. L. Huffaker, J Appl Phys, 105, 103104 (2009).

[7] S. H. Huang, G. Balakrishnan, A. Khoshakhagh, A. Jallipali, L. R. Dawson and D. L. Huffaker, Appl Phys Lett 88 131911 (2006).

[8] K. Akahane, N. Yamamoto, S. Gozu, A. Ueta, N. Ohtani, J. Cryst. Growth, 283, 297 (2005).

[9] Y. H. Kim and J. Y. Lee, Appl Phys Lett, 88, 241907 (2006).

[10] S. H. Vajargah, M. Couillard, K. Cui, S. G. Tavakoli, B. Robinson, R. N. Kleiman, J. S. Preston and G. A. Botton, Appl Phys Lett 98, 082113 (2011).

[11] S. H. Vajargah, S. Ghanad-Tavakoli, J. S. Preston, R. N. Kleiman and G. A. Botton, J. Appl. Phys, 114, 113101(2013).

[12] L. Cerutti, J. B. Rogriduez and E. Tournie, IEEE Photonics Technology Letters, 22, 8 (2010).

[13] J. R. Reboul, L. Cerutti, J. B. Rodriguez, P. Grech and E. Tournie, Appl Phys Lett, 99, 121113 (2011).

[14] A. Lee, H. Liu and A. Seeds, Semicond. Sci. Technol. 015027 (2013).

[15] G. Balakrishnan, S.H. Huang, A. Khoshakhlagh, A. Jallipalli, P. Rotella, A. Amtout, S. Krishna, C.P. Haines, L.R. Dawson and D.L. Huffaker, Electron. Lett. 42, 6 (2006).

[16] V. Srinivasan, V. K. Pamula and R. B. Fair, Lab Chip, 4, 310 (2004).

[17] J. B. Rodriguez, L. Cerutti, and E. Tournié, Appl. Phys. Lett 94, 023506 (2009).

[18] M. Mehta, G. Balakrishnan, S. Huang, A. Khoshakhlagh, A. Jallipalli, P. Patel, M. N. Kutty, L. R. Dawson, and D. L. Huffaker, Appl. Phys. Lett. 89, 211110 (2006).

[19] K. C. Nunna, S. L. Tan, C. J. Reyner, A. R. J. Marshall, B. Liang, A. Jallipalli, J. P. R. David, and D. L. Huffaker, IEEE Photonics Technol. Lett. 24, 3 (2012).

[20] S. P. Watkins, R. Arès, G. Soerensen, W. Zhong, C. A. Tran, J. E. Bryce and C. R. Bolognesi, J. Cryst. Growth, 170, 788 (1997).

[21] web-page of Ioffe at http://www.ioffe.ru/SVA/NSM/Semicond/

[22] S. Sridaran, A. Chavan and P. S. Dutta, J. Cryst. Growth 310, 1590 (2008).

[23] K.-M. Ko, J.-H. Seo, D.-E. Kim, S.-T. Lee, Y.-K. Noh, M.-D. Kim and J.-E. Oh, Nanotechnology, 20 225201 (2009).

[24] H. Liu, T. Wang, Q. Jiang, R. Hogg, F. Tutu, F. Pozzi and A. Seeds, Nature Photon. 5, 416–419 (2011).

[25] J. B. Rodriguez, L. Cerutti, P. Grech, G. Boissier, G. Narcy and E. Tournie, Proc. SPIE 7616, 76160V-1 (2010).

[26] S. M. Sze, Physics of Semiconductor Devices, 2nd ed. (Wiley Interscience, New York, 1981).

[27] P. S. Dutta, H. L. Bhat and V. Kumar, J. Appl. Phys. 81, 9 (1997).